Cumulant expansion in gluon saturation and five- and six-gluon azimuthal correlations

Şener Özönder[*]

Department of Physics, Istanbul Technical University, 34469 Istanbul, Turkey
and Department of Physics, Koc University, 34450 Istanbul, Turkey

Correlations between the momenta of the final state hadrons measured in proton or nucleus collisions contain information that sheds light on the initial conditions and evolutionary dynamics of the collision system. These correlation measurements have revealed the long-range rapidity correlations in p-p and p-Pb systems, and they have also made it possible to extract the elliptic flow coefficient from hadron correlation measurements. In this work, we calculate five- and six-gluon correlation functions in the framework of saturation physics by using superdiagrams. We also derive the cumulant expansion of the gluon correlators that is valid in the gluon saturation limit. We show that the cumulant expansion of the gluon correlators that is used for counting the number of diagrams to be calculated does not follow the standard cumulant expansion. We also explain how these findings can be used in obtaining experimentally relevant observables such as flow coefficients calculated from correlations as well as ratios of the correlation functions of different orders.

I. INTRODUCTION

The measured correlations between the final state hadrons in collisions involving protons and nuclei contain information about the dynamics of the collision and evolution of the produced particles [1]. In nucleus-nucleus (A-A) collisions, it has been observed that the particle pairs with the azimuthal angles ϕ_1 and ϕ_2 are maximally correlated when $\phi_1 - \phi_2 \sim 0$ (collimation) and $\phi_1 - \phi_2 \sim \pi$ (anticollimation) [2]. Also, this correlation is maintained even if the pair is separated by several units of rapidity. Such long-range azimuthal correlations in A-A collisions have been ascribed to the collective radial flow of the quark-gluon plasma [3]. Radial flow gives rise to collectivity in the hadronic spectrum where the momenta of the detected hadrons are not random but correlated.

In small systems such as p-p and p-A, the collectivity in the produced hadrons had not been observed in experiments or Monte Carlo simulations. Also, on the theory side there was no such expectation of collectivity in p-p and p-A collisions, since it had been thought that fluid behavior would not emerge in such small collision systems. However, the two-particle correlation measurements in p-p collisions at $\sqrt{s} = 7$ GeV at the LHC revealed for the first time the existence of collimation and anticollimation effects, which are long ranged in rapidity, appearing at high-multiplicity events—the so-called *double ridge* [4–7]. Later, the same ridge has also been seen in p-A collisions [8–15]. Afterwards, we predicted the existence of higher-dimensional ridges that would appear in three-, four-, and higher-dimensional particle correlation functions [16].

The observation of collectivity in p-p and p-Pb collisions later sparked an interest in applying hydrodynamics to such small systems [17–22]. An alternative program that we pursue in this work, however, does not assume hydrodynamical evolution. Instead, our approach here tracks the origin of the collectivity in small systems to gluon saturation in the target and projectile in p-p or p-A collisions [23–31]. Gluon saturation is expected to increase with increasing beam energy. Therefore, that ridge correlations appear only at high-multiplicity events at top LHC energies seems to be evidence supporting the onset of gluon saturation. The way gluon saturation affects particle production in proton or nucleus collisions is studied via glasma diagrams. Such calculations indicate that the two-hadron correlation function calculated from the glasma diagrams explains the systematics of the ridge signal at the LHC data [32–37].

Whether the origin of the collectivity observed in experiments is due to hydrodynamic evolution of the system or due to gluon saturation is still under discussion. The two-hadron correlations alone are not enough to settle this dispute. For this purpose, correlations between more than two hadrons must be measured, and these measurements need to be compared with the results from hydrodynamics and glasma diagrams separately [16,38].

Hadron correlation measurements are used to obtain the flow coefficients $v_m\{n\text{PC}\}$, where nPC refers to that the flow coefficient is found from n-particle correlations [39–41]. Currently, the elliptic flow coefficient v_2 is measured from $n = 2$, 4, 6, and 8 particles in experiments [42–45]. On the theory side, such coefficients can be calculated from glasma diagrams. By using glasma

[*]ozonder@uw.edu

diagrams, one can calculate the correlations of n gluons, and convolving these with the fragmentation functions results in the hadronic correlation functions that can be compared with the ones measured by the experiments. In this work, we calculate five- and six-gluon correlation functions from glasma superdiagrams towards this goal.

Another important result of this paper, in addition to the derivation of these two correlation functions, is the cumulant expansion of the gluon correlation functions in the gluon saturation limit. An n-gluon correlation function is a cumulant that can be expanded in terms of lower-order cumulants and nth moment [see, for example, Eq. (1)]. However, the standard cumulant expansion needs to be modified if one wants to use it to determine the number of glasma diagrams to be calculated. This has been realized for the first time in the calculation of four-gluon correlation function in Ref. [16]. Here we derive the formula that generates the modified cumulant expansion for the n-gluon correlation function obtained from the glasma diagrams. The importance of this modified cumulant expansion in the context of this work is to find the number of glasma diagrams to be calculated at a given order and use it to verify independently that the number of terms in the general formula that produces the correlation function at nth order is correct.

In the next section, we derive for the first time the formula that generates the modified cumulant expansion. Then, we review the recipe developed in Ref. [38] that yields the n-gluon correlation function. Following that, we will derive the five- and six-gluon correlation functions and verify by using the modified cumulant expansion that the number of terms, each of which corresponds to a connected glasma diagram, in these correlation functions is correct.

II. CUMULANT EXPANSION FOR RAINBOW GLASMA DIAGRAMS

The three- and four-gluon azimuthal correlation functions with full rapidity and transverse momentum dependence have been calculated in Ref. [16] by using 16 and 96 glasma diagrams, respectively. The observable to be calculated—and later compared to the experimentally obtained correlation function—for n gluons is the connected azimuthal correlation function C_n. Since this function includes only the connected diagrams, it is a cumulant, not a moment.

The number of connected diagrams to be calculated can be determined via the cumulant expansion. An important realization has been made that the glasma correlation functions at higher orders, starting with the four-gluon correlation function, obeyed the standard cumulant expansion, but one had to modify this expansion if it was to be used to determine the number of glasma diagrams at that order [16]. Hence, the cumulant expansion should be modified for the rainbow glasma diagrams when it is to be used to count glasma diagrams. To illustrate via the

example of a four-gluon correlation function, we first write the *standard* cumulant expansion at the fourth order:

$$\kappa_4 = \mu_4 - 4\kappa_3\kappa_1 - 3\kappa_2^2 - 6\kappa_2\kappa_1^2 - \kappa_1^4, \qquad (1)$$

where κ's denote the cumulants (connected correlations) and μ_4 denotes the fourth moment, which includes all connected and disconnected glasma diagrams involving four gluons. The number of glasma diagrams that each term contains is given by $\mu_4 = 209$, $\kappa_3 = 16$, $\kappa_2 = 4$, and $\kappa_1 = 1$ [16]. From this, we find $\kappa_4 = 72$, which is incorrect, since we know that one needs to calculate 96 connected rainbow glasma diagrams instead of 72 as explained in detail in Ref. [16]. This error occurs since in Eq. (1) the term $3\kappa_2^2 = 3(\kappa_2^{\text{up}} + \kappa_2^{\text{low}}) \otimes (\kappa_2^{\text{up}} + \kappa_2^{\text{low}})$ mixes the upper and lower glasma diagrams (see Fig. 1). The subtraction of the two mixed terms, $\kappa_2^{\text{up}} \otimes \kappa_2^{\text{low}}$ and $\kappa_2^{\text{low}} \otimes \kappa_2^{\text{up}}$, gives rise to wrong counting, since in the leading rainbow glasma approximation such diagrams are already never considered.

In other words, the moment μ_4 already does not contain such correlations, so one should not attempt to subtract the mixed diagrams ($\kappa_2^{\text{up}} \otimes \kappa_2^{\text{low}}$ and $\kappa_2^{\text{low}} \otimes \kappa_2^{\text{up}}$) from μ_4. Only the terms $\kappa_2^{\text{up}} \otimes \kappa_2^{\text{up}} + \kappa_2^{\text{low}} \otimes \kappa_2^{\text{low}}$ should be subtracted from μ_4. Considering that there are the same number of mixed (up $\otimes$ low and low $\otimes$ up) and unmixed (up $\otimes$ up and low $\otimes$ low) glasma diagrams and that we want to keep only the unmixed ones, we can simply substitute $3\kappa_2^2$ in Eq. (1) with $3\kappa_2^2/2$ and write the rainbow cumulant for rainbow glasma diagrams as[1]

$$\kappa_4 = \mu_4 - 4\kappa_3\kappa_1 - 3\frac{\kappa_2^2}{2} - 6\kappa_2\kappa_1^2 - \kappa_1^4. \qquad (2)$$

This gives the correct counting $\kappa_4 = 96$, which matches the number of connected diagrams calculated explicitly in Ref. [16]. The rainbow cumulant in the fifth order is written as

$$\kappa_5 = \mu_5 - 5\kappa_4\kappa_1 - 10\frac{\kappa_3\kappa_2}{2} - 10\kappa_3\kappa_1^2 - 15\frac{\kappa_2^2}{2}\kappa_1 - 10\kappa_2\kappa_1^3 - \kappa_1^5, \qquad (3)$$

and at the sixth order it is written as

$$\kappa_6 = \mu_6 - 6\kappa_5\kappa_1 - 15\frac{\kappa_4\kappa_2}{2} - 15\kappa_4\kappa_1^2 - 10\frac{\kappa_3^2}{2} - 60\frac{\kappa_3\kappa_2}{2}\kappa_1$$

$$- 20\kappa_3\kappa_1^3 - 15\frac{\kappa_2^3}{4} - 45\frac{\kappa_2^2}{2}\kappa_1^2 - 15\kappa_2\kappa_1^4 - \kappa_1^6. \qquad (4)$$

---

[1] We shall not add any specific identifier index for the rainbow cumulants to distinguish them from the standard ones; the rainbow cumulants are recognized by the 2's in the denominators of some of its terms in the expansion.
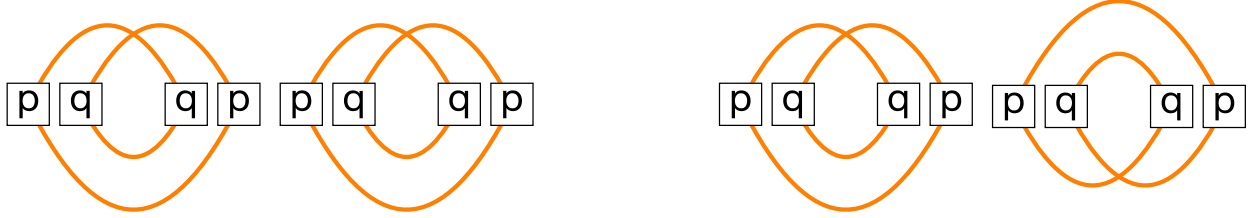
FIG. 1. Rainbow approximation refers to that either the upper or lower part of the diagrams includes lines that connect the same momentum labels ($p \leftrightarrow p$, $q \leftrightarrow q$, etc.). The four diagrams here separately satisfy this condition. Rainbow approximation, however, also requires that, when separate diagrams are combined as in $\kappa_2 \otimes \kappa_2$ in Eq. (1), all combined diagrams should have their rainbow parts in either their upper or lower parts. The two disconnected diagrams on the left are for the term $\kappa_2^{\text{low}} \otimes \kappa_2^{\text{low}}$, which is a rainbow diagram altogether. Therefore, this pair of diagrams is required to be subtracted from the moment μ. However, the pair on the right ($\kappa_2^{\text{low}} \otimes \kappa_2^{\text{up}}$) mixes lower and upper rainbow diagrams. Such terms are already nonexistent in the fourth moment μ_4, so subtracting such diagrams would lead to wrong counting.

Now we will derive the formula for the rainbow cumulants. The standard moment of the order of n in terms of cumulants is given in terms of the partial Bell polynomials $B_{n,k}$:

$$\mu_n = \sum_{k=1}^{n} B_{n,k}(\kappa_1, \kappa_2, \ldots, \kappa_{n-k+1}), \qquad (5)$$

and standard κ_n is found by solving this equation for κ_n. From the discussions above, we can write the expression for the rainbow moment as[2]

$$\mu_n = -\kappa_1^n + 2 \sum_{k=1}^{n} B_{n,k}\left(\kappa_1, \frac{\kappa_2}{2}, \ldots, \frac{\kappa_{n-k+1}}{2}\right), \qquad (6)$$

and the rainbow cumulant κ_n is found by solving this equation for κ_n. The formula in Eq. (6) is the first result of this paper.[3] After we derive the five- and six-gluon correlation functions later in this work, we will use the rainbow cumulant expansion in Eq. (6) to check if the five- and six-gluon correlation functions include the correct number of terms, where each term corresponds to one connected diagram.

III. FORMULA OF n-GLUON CORRELATION FUNCTION

In Ref. [38], we derived the formula for the n-gluon correlation function C_n with full momentum and rapidity dependence by using the glasma superdiagrams we developed. Here we quote the formulas that we will use in the next section to derive five- and six-gluon correlation functions.

The n-gluon correlation function is given by

$$C_n = \frac{\alpha_s^n N_c^n S_\perp}{\pi^{4n}(N_c^2-1)^{2n-1}} \left(\prod_{i=1}^{n}\frac{1}{p_{\perp i}^2}\right) \int \frac{d^2 k_\perp}{(2\pi)^2}(\mathcal{N}_1 + \mathcal{N}_2). \qquad (7)$$

Here α_s is the QCD strong coupling constant, $N_c = 3$ is the gluon color factor, $S_\perp$ is the transverse area of overlap during the collision between the target and projectile, and $p_{\perp i}$ are the transverse momentum variables of the gluons produced. $\mathcal{N}_{1,2}$, which include the unintegrated gluon distribution (UGD) functions $\Phi_{A,p}(p_\perp)$, are given by[4]

$$\mathcal{N}_1 = f_n \Phi_{1,p_1}^2(k_\perp) \left[\prod_{j=1}^{n-3}\Phi_{1,p_{j+1}}(k_\perp)\right] \left[\sum_{h=1}^{n-2} 2h\Phi_{1,p_{h+1}}(k_\perp)\right] \Phi_{2,p_1}(p_{\perp 1}-k_\perp)\mathcal{N}_{A_2}, \qquad (8)$$

$$\mathcal{N}_2 = f_n \Phi_{2,p_n}^2(k_\perp) \left[\prod_{j=1}^{n-3}\Phi_{2,p_{n-j}}(k_\perp)\right] \left[\sum_{h=1}^{n-2} 2h\Phi_{2,p_{n-h}}(k_\perp)\right] \Phi_{1,p_1}(p_{\perp 1}-k_\perp)\mathcal{N}_{A_1}, \qquad (9)$$

---

[2]The *Mathematica* code for both the standard and rainbow cumulants are given in the Appendix.

[3]To emphasize, the nonstandard, rainbow cumulant expansion is developed here for correctly counting the glasma diagrams. The correlation functions C_n still obey the standard cumulant expansion. This can be understood from the discussion following Eq. (46) in Ref. [16]. Equation (46) therein is clearly in the form of a standard cumulant expansion at the order of $n = 4$.

[4]The formulas for $\mathcal{N}_{1,2}$ given in Ref. [38] included a typo and missed the prefactor f_n, and the prefactor in the second brackets mistakenly read 2^h instead of $2h$. These mistakes in Ref. [38] originated from the miscalculation of the κ_5 therein.

where

$$\mathcal{N}_{A_1(A_2)} = \prod_{m=2}^{n} [\Phi_{1(2),p_m}(\boldsymbol{p}_{\perp m} - \boldsymbol{k}_\perp) + \Phi_{1(2),p_m}(\boldsymbol{p}_{\perp m} + \boldsymbol{k}_\perp)]. \tag{10}$$

The indices of $\Phi_{A,p}(\boldsymbol{p}_\perp)$ are as follows. A stands for the target or projectile index ($A = 1, 2$), p subscript is the rapidity variable of the gluon, and $\boldsymbol{p}_\perp$ is the transverse momentum variable of the gluon.

The coefficient f_n is given by

$$f_n = \begin{cases} 1 & \text{if } n < 5, \\ (n-3)! & \text{if } n \geq 5, \end{cases} \tag{11}$$

where n here is the same n as in C_n, i.e., number of gluons.

It is important to note that the rapidity indices and that which UGD appears with which prefactor in the formulas above are nontrivial. The former is found by means of superdiagrams, and the latter is found by means of the rainbow cumulant expansion. In this work, we will show only the relevant superdiagrams for C_5 and C_6, but we will not explain how they are drawn, for which we refer the interested reader to our earlier work [38].

IV. FIVE-GLUON AZIMUTHAL CORRELATION FUNCTION

The five-gluon correlation function C_5 can be written by using the formulas given in Eqs. (7)–(10) as follows:

$$C_5(\boldsymbol{p},\boldsymbol{q},\boldsymbol{l},\boldsymbol{w},\boldsymbol{r}) = \frac{\alpha_s^5 N_c^5 S_\perp}{\pi^{20}(N_c^2-1)^9} \frac{1}{\boldsymbol{p}_\perp^2 \boldsymbol{q}_\perp^2 \boldsymbol{l}_\perp^2 \boldsymbol{w}_\perp^2 \boldsymbol{r}_\perp^2} \int \frac{d^2\boldsymbol{k}_\perp}{(2\pi)^2} (\mathcal{N}_1^{(5)} + \mathcal{N}_2^{(5)}), \tag{12}$$

where

$$\mathcal{N}_1^{(5)} = 2\Phi_{1,p}^2(\boldsymbol{k}_\perp)\Phi_{1,q}(\boldsymbol{k}_\perp)\Phi_{1,l}(\boldsymbol{k}_\perp)[2\Phi_{1,q}(\boldsymbol{k}_\perp) + 4\Phi_{1,l}(\boldsymbol{k}_\perp) + 6\Phi_{1,w}(\boldsymbol{k}_\perp)]\Phi_{2,p}(\boldsymbol{p}_\perp - \boldsymbol{k}_\perp)\mathcal{N}_{A_2}^{(5)}, \tag{13}$$

$$\mathcal{N}_2^{(5)} = 2\Phi_{2,r}^2(\boldsymbol{k}_\perp)\Phi_{2,w}(\boldsymbol{k}_\perp)\Phi_{2,l}(\boldsymbol{k}_\perp)[2\Phi_{2,w}(\boldsymbol{k}_\perp) + 4\Phi_{2,l}(\boldsymbol{k}_\perp) + 6\Phi_{2,q}(\boldsymbol{k}_\perp)]\Phi_{1,p}(\boldsymbol{p}_\perp - \boldsymbol{k}_\perp)\mathcal{N}_{A_1}^{(5)}, \tag{14}$$

and

$$\mathcal{N}_{A_1(A_2)}^{(5)} = [\Phi_{1(2),q}(\boldsymbol{q}_\perp - \boldsymbol{k}_\perp) + \Phi_{1(2),q}(\boldsymbol{q}_\perp + \boldsymbol{k}_\perp)][\Phi_{1(2),l}(\boldsymbol{l}_\perp - \boldsymbol{k}_\perp) + \Phi_{1(2),l}(\boldsymbol{l}_\perp + \boldsymbol{k}_\perp)]$$
$$\times [\Phi_{1(2),w}(\boldsymbol{w}_\perp - \boldsymbol{k}_\perp) + \Phi_{1(2),w}(\boldsymbol{w}_\perp + \boldsymbol{k}_\perp)][\Phi_{1(2),r}(\boldsymbol{r}_\perp - \boldsymbol{k}_\perp) + \Phi_{1(2),r}(\boldsymbol{r}_\perp + \boldsymbol{k}_\perp)]. \tag{15}$$

The nth level moment μ_n includes both the connected and disconnected glasma diagrams for n-gluon correlation functions, and it is given by $\mu_n = 2(2n-1)!! - 1$. Using Eq. (3) and that $\mu_5 = 1889$, $\kappa_1 = 1$, $\kappa_2 = 4$, $\kappa_3 = 16$, and $\kappa_4 = 96$, one finds $\kappa_5 = 768$. So, one needs to consider 768 connected glasma diagrams to calculate C_5. Equation (15) has 2^4 terms, so Eq. (13) contains $2 \times (2 + 4 + 6) \times 2^4 = 384$ terms. Similarly, Eq. (14) contains 384 terms as well.

So, C_5 in Eq. (12) includes exactly 768 terms, which matches with the number that we find from the rainbow cumulant expansion.

It would be practically impossible to calculate such number of diagrams separately without the superdiagrams, where one needs only three superdiagrams for C_5 (see Fig. 2). For C_6, one needs to calculate 7680 connected glasma diagrams or only four superdiagrams.
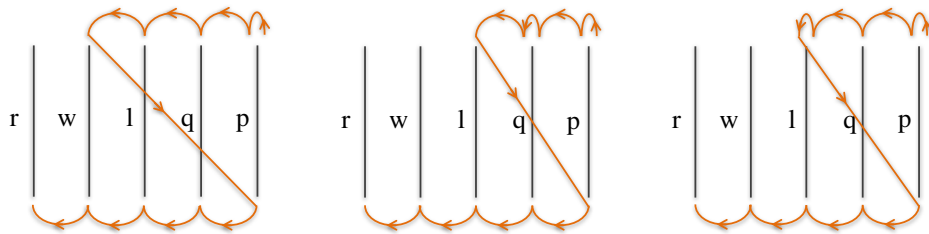

FIG. 2. Superdiagrams for C_5. These three superdiagrams give rise to $\mathcal{N}_1^{(5)}$ in Eq. (13), particularly the rapidity indices of the unintegrated distribution functions Φ. There are three other superdiagrams that are diagonally mirror images of these; i.e., they run starting from the bottom left and end at the top right. Those diagrams give $\mathcal{N}_2^{(5)}$ in Eq. (14).
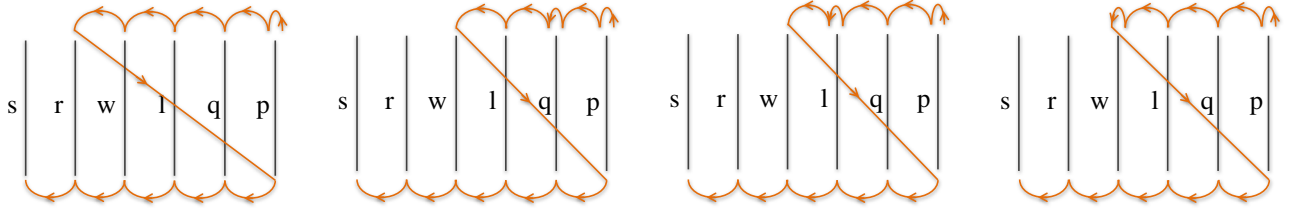
FIG. 3. Superdiagrams for C_6. These four superdiagrams give rise to $\mathcal{N}_1^{(6)}$ in Eq. (17). There are four other superdiagrams that are diagonally mirror images of these; i.e., they run starting from the bottom left and end at the top right. Those diagrams give $\mathcal{N}_2^{(6)}$ in Eq. (18).

V. SIX-GLUON AZIMUTHAL CORRELATION FUNCTION

The six-gluon correlation function C_6 can be written by using the formulas given in Eqs. (7)–(10) as follows:

$$C_6(\boldsymbol{p},\boldsymbol{q},\boldsymbol{l},\boldsymbol{w},\boldsymbol{r},\boldsymbol{s}) = \frac{\alpha_s^6 N_c^6 S_\perp}{\pi^{24}(N_c^2-1)^{11}} \frac{1}{p_\perp^2 q_\perp^2 l_\perp^2 w_\perp^2 r_\perp^2 s_\perp^2} \int \frac{d^2\boldsymbol{k}_\perp}{(2\pi)^2} (\mathcal{N}_1^{(6)} + \mathcal{N}_2^{(6)}), \tag{16}$$

where

$$\mathcal{N}_1^{(6)} = 6\Phi_{1,p}^2(\boldsymbol{k}_\perp)\Phi_{1,q}(\boldsymbol{k}_\perp)\Phi_{1,l}(\boldsymbol{k}_\perp)\Phi_{1,w}(\boldsymbol{k}_\perp)[2\Phi_{1,q}(\boldsymbol{k}_\perp) + 4\Phi_{1,l}(\boldsymbol{k}_\perp) + 6\Phi_{1,w}(\boldsymbol{k}_\perp) + 8\Phi_{1,r}(\boldsymbol{k}_\perp)]$$
$$\times \Phi_{2,p}(\boldsymbol{p}_\perp - \boldsymbol{k}_\perp)\mathcal{N}_{A_2}^{(6)}, \tag{17}$$
$$\mathcal{N}_2^{(6)} = 6\Phi_{2,s}^2(\boldsymbol{k}_\perp)\Phi_{2,r}(\boldsymbol{k}_\perp)\Phi_{2,w}(\boldsymbol{k}_\perp)\Phi_{2,l}(\boldsymbol{k}_\perp)[2\Phi_{2,r}(\boldsymbol{k}_\perp) + 4\Phi_{2,w}(\boldsymbol{k}_\perp) + 6\Phi_{2,l}(\boldsymbol{k}_\perp) + 8\Phi_{1,q}(\boldsymbol{k}_\perp)]$$
$$\times \Phi_{1,p}(\boldsymbol{p}_\perp - \boldsymbol{k}_\perp)\mathcal{N}_{A_1}^{(5)}, \tag{18}$$

and

$$\mathcal{N}_{A_1(A_2)}^{(6)} = [\Phi_{1(2),q}(\boldsymbol{q}_\perp - \boldsymbol{k}_\perp) + \Phi_{1(2),q}(\boldsymbol{q}_\perp + \boldsymbol{k}_\perp)][\Phi_{1(2),l}(\boldsymbol{l}_\perp - \boldsymbol{k}_\perp) + \Phi_{1(2),l}(\boldsymbol{l}_\perp + \boldsymbol{k}_\perp)]$$
$$\times [\Phi_{1(2),w}(\boldsymbol{w}_\perp - \boldsymbol{k}_\perp) + \Phi_{1(2),w}(\boldsymbol{w}_\perp + \boldsymbol{k}_\perp)][\Phi_{1(2),r}(\boldsymbol{r}_\perp - \boldsymbol{k}_\perp) + \Phi_{1(2),r}(\boldsymbol{r}_\perp + \boldsymbol{k}_\perp)]$$
$$\times [\Phi_{1(2),s}(\boldsymbol{s}_\perp - \boldsymbol{k}_\perp) + \Phi_{1(2),s}(\boldsymbol{s}_\perp + \boldsymbol{k}_\perp)]. \tag{19}$$

Using Eq. (4) and that $\mu_6 = 2(2 \times 6 - 1)!! - 1 = 20789$, $\kappa_1 = 1$, $\kappa_2 = 4$, $\kappa_3 = 16$, $\kappa_4 = 96$, and $\kappa_5 = 768$, one finds $\kappa_6 = 7680$. C_6 in Eq. (16) includes exactly 7680 terms, so this verifies that Eq. (16) is correct. The superdiagrams needed for calculating C_6 are given in Fig. 3.

VI. CONCLUSION

In this paper, we derived the modified cumulant expansion that was to be used for counting glasma diagrams correctly. This expansion is essential in deriving the correlation functions and verifying that they are found from the correct glasma diagrams. We also derived the five- and six-gluon correlation functions. The six-gluon correlation function, particularly, can be used to calculate the elliptic flow $v_2\{6\}$, and then it can be compared with the measurements. Another use of the correlation functions we calculated could be studying correlations between flow coefficients [46] as well

as obtaining other observables from the ratios of the cumulants (C_n's) [47]. These studies are under way.

APPENDIX: CODES FOR THE CUMULANTS IN MATHEMATICA

The *Mathematica* function which gives the standard cumulant expansion of κ_n is [see Eq. (5)]

$$\kappa[n\_] := \kappa_n + \mu_n - \sum_{k=1}^{n} \text{BellY}[n, k, \text{Table}[\kappa_m, \{m, n\}]], \tag{A1}$$

and that which gives the rainbow cumulant expansion of κ_n is [see Eq. (6)]

$$\kappa[n_-] := \kappa_1^n + \kappa_n + \mu_n - 2 \sum_{k=1}^{n} \text{BellY}\left[n, k, \text{Join}\left[\{\kappa_1\}, \text{Table}\left[\frac{\kappa_m}{2}, \{m, 2, n\}\right]\right]\right]. \tag{A2}$$

[1] P. Di Francesco, M. Guilbaud, M. Luzum, and J.-Y. Ollitrault, Systematic procedure for analyzing cumulants at any order, Phys. Rev. C **95**, 044911 (2017).

[2] F. Wang, Dihadron correlations relative to the event plane in 200 GeV Au + Au collisions from STAR, J. Phys. Conf. Ser. **458**, 012029 (2013).

[3] A. Dumitru, F. Gelis, L. McLerran, and R. Venugopalan, Glasma flux tubes and the near side ridge phenomenon at RHIC, Nucl. Phys. **A810**, 91 (2008).

[4] V. Khachatryan et al., Observation of long-range near-side angular correlations in proton-proton collisions at the LHC, J. High Energy Phys. 09 (2010) 091.

[5] D. Velicanu, Ridge correlation structure in high multiplicity pp collisions with CMS, J. Phys. G **38**, 124051 (2011).

[6] W. Li, Observation of a "Ridge" correlation structure in high multiplicity proton-proton collisions: A brief review, Mod. Phys. Lett. A **27**, 1230018 (2012).

[7] K. W. Wozniak, Study of the long-range azimuthal correlations in pp and $p + Pb$ collisions with the ATLAS detector at the LHC, J. Phys. Conf. Ser. **779**, 012057 (2017).

[8] S. Chatrchyan et al., Observation of long-range near-side angular correlations in proton-lead collisions at the LHC, Phys. Lett. B **718**, 795 (2013).

[9] B. Abelev et al., Long-range angular correlations on the near and away side in p-Pb collisions at $\sqrt{s_{NN}} = 5.02$ TeV, Phys. Lett. B **719**, 29 (2013).

[10] G. Aad et al., Observation of Associated Near-Side and Away-Side Long-Range Correlations in $\sqrt{s_{NN}} = 5.02$ TeV Proton-Lead Collisions with the ATLAS Detector, Phys. Rev. Lett. **110**, 182302 (2013).

[11] L. Milano, Long-range angular correlations at the LHC with ALICE, Nucl. Phys. **A931**, 1017 (2014).

[12] B. B. Abelev et al., Long-range angular correlations of pi, K and p in p-Pb collisions at $\sqrt{s_{NN}} = 5.02$ TeV, Phys. Lett. B **726**, 164 (2013).

[13] B. B. Abelev et al., Multiparticle azimuthal correlations in p-Pb and Pb-Pb collisions at the CERN Large Hadron Collider, Phys. Rev. C **90**, 054901 (2014).

[14] B. B. Abelev et al., Multiplicity dependence of jet-like two-particle correlation structures in p-Pb collisions at $\sqrt{s_{NN}} = 5.02$ TeV, Phys. Lett. B **741**, 38 (2015).

[15] G. Aad et al., Measurement of long-range pseudorapidity correlations and azimuthal harmonics in $\sqrt{s_{NN}} = 5.02$ TeV proton-lead collisions with the ATLAS detector, Phys. Rev. C **90**, 044906 (2014).

[16] S. Ozonder, Triple-gluon and quadruple-gluon azimuthal correlations from glasma and higher-dimensional ridges, Phys. Rev. D **91**, 034005 (2015).

[17] P. Bozek, Collective flow in p-Pb and d-Pd collisions at TeV energies, Phys. Rev. C **85**, 014911 (2012).

[18] P. Bozek and W. Broniowski, Correlations from hydrodynamic flow in p-Pb collisions, Phys. Lett. B **718**, 1557 (2013).

[19] P. Bozek, W. Broniowski, and G. Torrieri, Mass Hierarchy in Identified Particle Distributions in Proton-Lead Collisions, Phys. Rev. Lett. **111**, 172303 (2013).

[20] K. Werner, M. Bleicher, B. Guiot, Iu. Karpenko, and T. Pierog, Evidence for Flow in pPb Collisions at 5 TeV from v_2 Mass Splitting, Phys. Rev. Lett. **112**, 232301 (2014).

[21] I. Kozlov, M. Luzum, G. Denicol, S. Jeon, and C. Gale, Transverse momentum structure of pair correlations as a signature of collective behavior in small collision systems, arXiv:1405.3976.

[22] A. Bzdak and G.-L. Ma, Elliptic and Triangular Flow in $p + Pb$ and Peripheral Pb + Pb Collisions from Parton Scatterings, Phys. Rev. Lett. **113**, 252301 (2014).

[23] K. Dusling, F. Gelis, T. Lappi, and R. Venugopalan, Long range two-particle rapidity correlations in A + A collisions from high energy QCD evolution, Nucl. Phys. **A836**, 159 (2010).

[24] K. Dusling, D. Fernandez-Fraile, and R. Venugopalan, Three-particle correlation from glasma flux tubes, Nucl. Phys. **A828**, 161 (2009).

[25] A. Kovner, L. D. McLerran, and H. Weigert, Gluon production at high transverse momentum in the McLerran-Venugopalan model of nuclear structure functions, Phys. Rev. D **52**, 3809 (1995).

[26] Y. V. Kovchegov and D. H. Rischke, Classical gluon radiation in ultrarelativistic nucleus-nucleus collisions, Phys. Rev. C **56**, 1084 (1997).

[27] F. Gelis, T. Lappi, and L. McLerran, Glittering glasmas, Nucl. Phys. **A828**, 149 (2009).

[28] L. D. McLerran and R. Venugopalan, Computing quark and gluon distribution functions for very large nuclei, Phys. Rev. D **49**, 2233 (1994).

[29] L. D. McLerran and R. Venugopalan, Gluon distribution functions for very large nuclei at small transverse momentum, Phys. Rev. D **49**, 3352 (1994).

[30] L. D. McLerran and R. Venugopalan, Green's functions in the color field of a large nucleus, Phys. Rev. D **50**, 2225 (1994).

[31] Y. V. Kovchegov, Non-Abelian Weizsacker-Williams field and a two-dimensional effective color charge density for a very large nucleus, Phys. Rev. D **54**, 5463 (1996).

[32] A. Dumitru, K. Dusling, F. Gelis, J. Jalilian-Marian, T. Lappi, and R. Venugopalan, The ridge in proton-proton collisions at the LHC, Phys. Lett. B **697**, 21 (2011).

[33] K. Dusling and R. Venugopalan, Azimuthal Collimation of Long Range Rapidity Correlations by Strong Color Fields in High Multiplicity Hadron-Hadron Collisions, Phys. Rev. Lett. **108,** 262001 (2012).

[34] K. Dusling and R. Venugopalan, Evidence for BFKL and saturation dynamics from dihadron spectra at the LHC, Phys. Rev. D **87,** 051502 (2013).

[35] K. Dusling and R. Venugopalan, Explanation of systematics of CMS $p + Pb$ high multiplicity di-hadron data at $\sqrt{s_{NN}} = 5.02$ TeV, Phys. Rev. D **87,** 054014 (2013).

[36] K. Dusling and R. Venugopalan, Comparison of the color glass condensate to dihadron correlations in proton-proton and proton-nucleus collisions, Phys. Rev. D **87,** 094034 (2013).

[37] R. Venugopalan, Long range correlations in high multiplicity hadron collisions:building bridges with ridges, Ann. Phys. **352,** 108 (2015).

[38] Ş. Özönder, Long range azimuthal correlations of multiple gluons in gluon saturation limit, Phys. Rev. D **93,** 054036 (2016).

[39] A. Bilandzic, R. Snellings, and S. Voloshin, Flow analysis with cumulants: Direct calculations, Phys. Rev. C **83,** 044913 (2011).

[40] B. Schenke, Origins of collectivity in small systems, arXiv:1704.03914.

[41] K. Dusling, W. Li, and B. Schenke, Novel collective phenomena in high-energy proton-proton and proton-nucleus collisions, Int. J. Mod. Phys. E **25,** 1630002 (2016).

[42] J. Adam *et al.*, Pseudorapidity dependence of the anisotropic flow of charged particles in Pb-Pb collisions at $\sqrt{s_{NN}} = 2.76$ TeV, Phys. Lett. B **762,** 376 (2016).

[43] M. Aaboud *et al.*, Measurement of multi-particle azimuthal correlations with the subevent cumulant method in pp and $p + Pb$ collisions with the ATLAS detector at the LHC, arXiv:1708.03559.

[44] S. Padula, Measurements of flow and correlation phenomena in pp, pPb and PbPb collisions at CMS, *Proc. Sci.,* ICHEP2016 (2016) 358.

[45] R. Belmont, PHENIX results on multiparticle correlations in small systems, arXiv:1704.04570.

[46] J. Adam *et al.*, Correlated Event-by-Event Fluctuations of Flow Harmonics in Pb-Pb Collisions at $\sqrt{s_{NN}} = 2.76$ TeV, Phys. Rev. Lett. **117,** 182301 (2016).

[47] A. Bzdak and V. Koch, Rapidity dependence of proton cumulants and correlation functions, arXiv:1707.02640.